

On the accuracy of coherent modified Redfield theory in simulating excitation energy transfer dynamics

Yu Chang and Yuan-Chung Cheng

Citation: *The Journal of Chemical Physics* **142**, 034109 (2015); doi: 10.1063/1.4905721

View online: <http://dx.doi.org/10.1063/1.4905721>

View Table of Contents: <http://scitation.aip.org/content/aip/journal/jcp/142/3?ver=pdfcov>

Published by the [AIP Publishing](#)

Articles you may be interested in

[Criteria for the accuracy of small polaron quantum master equation in simulating excitation energy transfer dynamics](#)

J. Chem. Phys. **139**, 224112 (2013); 10.1063/1.4840795

[Energy-transfer and charge-separation pathways in the reaction center of photosystem II revealed by coherent two-dimensional optical spectroscopy](#)

J. Chem. Phys. **133**, 184501 (2010); 10.1063/1.3493580

[Unified treatment of coherent and incoherent electronic energy transfer dynamics using classical electrodynamics](#)

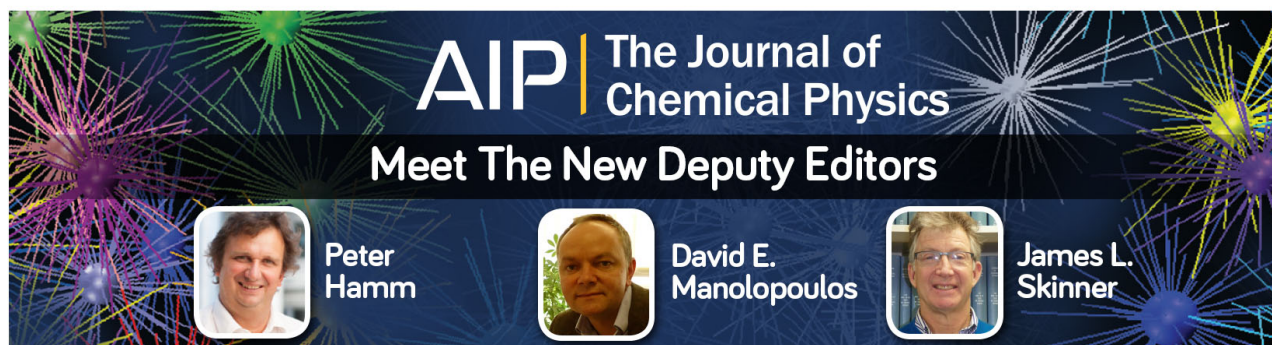
J. Chem. Phys. **133**, 144107 (2010); 10.1063/1.3488136

[Theory of coherent resonance energy transfer for coherent initial condition](#)

J. Chem. Phys. **131**, 164101 (2009); 10.1063/1.3247899

[Theory of coherent resonance energy transfer](#)

J. Chem. Phys. **129**, 101104 (2008); 10.1063/1.2977974



AIP | The Journal of
Chemical Physics

Meet The New Deputy Editors

	Peter Hamm		David E. Manolopoulos		James L. Skinner
---	-------------------	---	------------------------------	---	-------------------------

On the accuracy of coherent modified Redfield theory in simulating excitation energy transfer dynamics

Yu Chang and Yuan-Chung Cheng^{a)}

Department of Chemistry and Center for Quantum Science and Engineering, National Taiwan University, Taipei City 106, Taiwan

(Received 8 November 2014; accepted 29 December 2014; published online 16 January 2015)

In this study, we investigate the accuracy of a recently developed coherent modified Redfield theory (CMRT) in simulating excitation energy transfer (EET) dynamics. The CMRT is a secular non-Markovian quantum master equation that is derived by extending the modified Redfield theory to treat coherence dynamics in molecular excitonic systems. Herein, we systematically survey the applicability of the CMRT in a large EET parameter space through the comparisons of the CMRT EET dynamics in a dimer system with the numerically exact results. The results confirm that the CMRT exhibits a broad applicable range and allow us to locate the specific parameter regimes where CMRT fails to provide adequate results. Moreover, we propose an accuracy criterion based on the magnitude of second-order perturbation to characterize the applicability of CMRT and show that the criterion summarizes all the benchmark results and the physics described by CMRT. Finally, we employ the accuracy criterion to quantitatively compare the performance of CMRT to that of a small polaron quantum master equation approach. The comparison demonstrates the complementary nature of these two methods, and as a result, the combination of the two methods provides accurate simulations of EET dynamics for the full parameter space investigated in this study. Our results not only delicately evaluate the applicability of the CMRT but also reveal new physical insights for factors controlling the dynamics of EET that should be useful for developing more accurate and efficient methods for simulations of EET dynamics in molecular aggregate systems. © 2015 AIP Publishing LLC. [<http://dx.doi.org/10.1063/1.4905721>]

I. INTRODUCTION

Excitation energy transfer (EET) plays a crucial role in photosynthetic light harvesting. In natural photosynthesis, light energy captured in the antenna moves between pigments and finally reaches the reaction center to trigger charge separation.^{1,2} This process exhibits remarkable near unity quantum efficiency; therefore, understanding photosynthetic EET could provide means to improve artificial light-harvesting materials such as in the designs of solar cells and photosensitive conjugated polymers.^{3–5} To achieve this goal, theoretical methods that can adequately describe photosynthetic EET dynamics are necessary; however, this task has proven to be highly nontrivial.^{6–8} Photosynthetic systems often exhibit a broad distribution of inter-pigment interactions, energetic disorder, and a large number of pigments, making accurate theoretical description of EET dynamics a challenging task. Recent advances have shown that the traditional Förster and Redfield theories for EET cannot fully and adequately describe EET in photosynthetic systems.^{8–12}

To go beyond the traditional Förster and Redfield theories, studies based on non-perturbative methods,^{13–19} path-integral approaches,^{20–23} polaronic methods,^{24–28} and hybrid approaches^{12,22,29–31} have drawn intensive attentions recently. Among them, the so-called modified Redfield theory^{32,33} has been demonstrated to be a quite effective method for

photosynthetic EET.^{12,33–35} The modified Redfield theory is a second-order perturbative approach using the exciton-phonon interactions as the perturbation. The main idea behind this theory is to separate the diagonal part from the off-diagonal part of the exciton-phonon coupling Hamiltonian in the electronic eigen-basis (the so-called exciton basis) and then include the diagonal part in the zeroth-order Hamiltonian. By treating the diagonal exciton-phonon coupling exactly and the off-diagonal part perturbatively, the modified Redfield theory includes multiphonon effects and a smaller perturbation term, leading to its broader range of applicability when compared to the simple Redfield method.^{12,33–35} The modified Redfield theory has been successfully applied to describe EET dynamics and spectroscopy of many photosynthetic systems; however, a key limitation of the theory is that it considers only population transfer and does not describe coherent dynamics.

Motivated by the observation of long-lived quantum coherence in photosynthetic light-harvesting systems and conjugated polymer systems,³⁶ we have extended the idea of the modified Redfield theory to derive a quantum master equation that provides the equation of motion for the full reduced density matrix of an excitonic system.^{37,38} The result was a coherent modified Redfield theory (CMRT) that provides clear physical description for EET dynamics in a broad parameter regime and is computationally efficient compared with the higher-order perturbation theory and the numerically exact method. Moreover, we have shown that the CMRT method provides excellent descriptions of coherent EET dynamics in

^{a)}Electronic mail: yuanchung@ntu.edu.tw

a large parameter space.^{38,39} When compared to the reduced hierarchy equation approach, CMRT excellently describes the coherent dynamics in the Fenna-Matthews-Olson (FMO) complex.³⁷ Moreover, we expect that the CMRT can be applied to efficiently and accurately describe spectroscopy and EET dynamics in large photosynthetic systems, since the modified Redfield theory has shown promising success in this area.³⁴ Therefore, we believe that CMRT is a powerful approach to efficiently simulate EET dynamics in large and complicated systems. Nevertheless, since CMRT is a perturbative approach, it is critical that we can systematically assess its range of applicability in describing photosynthetic EET dynamics.

In the present study, we aim to evaluate the accuracy of CMRT in the parameter space of photosynthetic EET and explore physical parameters affecting EET dynamics. This will be useful for the realistic applications of the CMRT method, and a detailed understanding of the validity of the perturbative method could provide useful insights into the key factors controlling EET dynamics in different parameter regimes. This paper is organized as follows. In Sec. II, we present the Hamiltonian of a dimer model system adopted in this work and the theoretical background of CMRT. We then detail our results in Sec. III. To investigate the accuracy of CMRT, we carry out a comprehensive comparison of the results calculated by CMRT with those from the numerically exact quasi adiabatic path integral (QUAPI) method in various parameter regimes.⁴⁰ We then examine the compiled data to determine the applicability regimes of CMRT and to develop an accuracy criterion for the CMRT approach. In addition, we apply this criterion to quantitatively compare the performance of the CMRT approach to that of a polaronic quantum master equation approach, in order to shed light on how dynamical fluctuations of the environments affect EET dynamics. Finally, Sec. IV presents our main conclusions.

II. THEORY

A. Hamiltonian

Following the standard practice in treating EET problems, we adopt a standard Frenkel-exciton Hamiltonian to describe photoexcitations of molecular systems in the one-exciton manifold and consider independent harmonic baths coupled to the excitations localized on each individual chromophores. In the exciton basis, the full system plus bath Hamiltonian can be written as

$$H = H^{el} + H^{ph} + H^{el-ph},$$

where

$$H^{el} = \sum_{\alpha} \epsilon_{\alpha} |\alpha\rangle\langle\alpha|, \quad (1)$$

$$H^{ph} = \sum_n \sum_i \hbar\omega_{ni} \left(b_{ni}^{\dagger} b_{ni} + \frac{1}{2} \right), \quad (2)$$

and the system-bath coupling in the exciton basis reads

$$H^{el-ph} = \sum_{\alpha,\beta} |\alpha\rangle\langle\beta| \sum_n \sum_i C_n^{\alpha} C_n^{\beta} g_{ni} \hbar\omega_{ni} (b_{ni}^{\dagger} + b_{ni}). \quad (3)$$

Here, H^{el} is the electronic Hamiltonian of the system, where $|\alpha\rangle$ denotes a exciton state that can be represented as linear combinations of site-localized excited states, $|\alpha\rangle = \sum_n C_n^{\alpha} |n\rangle$, and ϵ_{α} is the transition energy of $|\alpha\rangle$. The term H^{ph} is the bath Hamiltonian, where b_{ni}^{\dagger} (b_{ni}) is the creation (annihilation) operator of the i th oscillator mode localized on site n , and ω_{ni} denotes the phonon frequency. Finally, the system-bath Hamiltonian H^{el-ph} represents bilinear exciton-phonon coupling diagonal in the site basis, where g_{ni} is the exciton-phonon coupling constant between $|n\rangle$ and the i th oscillator mode localized on site n . H^{el-ph} has off-diagonal matrix elements in the exciton basis due to the unitary transformation to the exciton basis.

To investigate the accuracy of CMRT, we considered EET in a simple dimer system. The system Hamiltonian in the site basis employed in this study is

$$H = \begin{bmatrix} -\Delta & J \\ J & \Delta \end{bmatrix}, \quad (4)$$

where 2Δ is the energy gap between the two site-localized excitations, and J is the electronic coupling between them. As condensed-phase systems are concerned, we used spectral density functions defined as

$$J_n(\omega) = \sum_i g_{ni}^2 \hbar^2 \omega_{ni}^2 \delta(\omega - \omega_{ni})$$

to describe the collective exciton-phonon couplings.⁴¹ In this study, we applied an identical super-ohmic-type spectral density to each site,

$$J_n(\omega) = \frac{\gamma\omega^3}{\pi\omega_c^2} \exp\left(-\frac{\omega}{\omega_c}\right), \quad (5)$$

where γ is the exciton-phonon coupling strength, and ω_c is the cutoff frequency of the phonon bath, which is used as the energy unit in the following calculations.

B. Coherent modified Redfield theory

The key idea of the original modified Redfield theory is to include the diagonal part of the exciton-phonon Hamiltonian (Eq. (3)) into the unperturbed zeroth-order Hamiltonian and treat only the off-diagonal part of the exciton-phonon Hamiltonian perturbatively. The modified Redfield theory is limited to population dynamics and Markovian rates, because coherence dynamics are ignored in its derivation.^{32,33} We had followed the same Hamiltonian partitioning and applied a second-order cumulant expansion approach to derive a quantum master equation for EET dynamics, which is called the coherent modified Redfield theory.^{37,38} We have previously applied this method to calculate EET dynamics for model photosynthetic systems to show that CMRT provides a framework with solid physical interpretations and high computational efficiency while retaining excellent accuracy

within a large EET parameter space. However, the full parameter range for the accuracy of the CMRT method has not been assessed. In this work, we aim to investigate the applicability of CMRT in simulating EET dynamics by comprehensive comparisons with numerically exact results in a broad parameter regime.

Herein, we briefly describe the equation of motion of CMRT and present a brief derivation of the theory in Appendix for the sake of completeness of this work. The CMRT approach is a non-Markovian secular quantum master equation that describes the time-evolution of the reduced density matrix of an exciton system in the exciton basis,

$$\begin{aligned} \dot{\sigma}_{\alpha\beta}(t) = & \frac{-i}{\hbar} [(\epsilon_{\alpha} - \lambda_{\alpha\alpha\alpha\alpha}) - (\epsilon_{\beta} - \lambda_{\beta\beta\beta\beta})] \sigma_{\alpha\beta}(t) \\ & + R_{\alpha\beta}^{pd}(t) \sigma_{\alpha\beta}(t) \\ & + \sum_f [R_{\alpha f}(t) \sigma_{ff}(t) - R_{f\alpha}(t) \sigma_{\alpha\alpha}(t)] \delta_{\alpha\beta} \\ & - \frac{1}{2} \sum_f [R_{f\alpha}(t) + R_{f\beta}(t)] \sigma_{\alpha\beta}(t). \end{aligned} \quad (6)$$

The first two terms in Eq. (6) describe the coherent dynamics and pure dephasing driven by the zeroth-order Hamiltonian, respectively. $\lambda_{\alpha\alpha\alpha\alpha} = \sum_n |C_n^{\alpha}|^4 \lambda_n$ is the reorganization energy of the exciton state $|\alpha\rangle$, λ_n is the site reorganization energy of the n th site, $\lambda_n = \int_0^{\infty} d\omega J_n(\omega)/\omega$, and $R_{\alpha\beta}^{pd}(t)$ is the non-Markovian pure-dephasing rate given by Eq. (A10). The last two terms in Eq. (6) describe the dissipative dynamics including population transfers and population induced dephasing of the coherences, where $R_{\alpha\beta}(t)$ is the time-dependent population transfer rate from $|\beta\rangle$ to $|\alpha\rangle$ that can be evaluated from spectral densities (Eq. (A16)). CMRT not only retains the coherence dynamics in the quantum master equation but also discards the Markovian approximation used in the original modified Redfield theory in order to partially capture the bath memory effects to ensure the accuracy of short time dynamics in the propagation of the CMRT. Note that Eq. (6) is of a time-convolution-less form, and as a result some bath memory effects that can only be captured by a time-convoluted equation are not described in the CMRT method. Nevertheless, in the CMRT approach, the rate tensor is still time dependent; therefore, we state that the CMRT approach is a non-Markovian quantum master equation. We found that the non-Markovian form plays a critical role in solving the problem of positivity violation

in the short-time dynamics, as pointed out previously by Suarez *et al.*^{42,43} Therefore, we remark that the secular, non-Markovian form of the CMRT equation of motion significantly reduces the problem of positivity violation as compared to the Markovian version.

III. RESULTS AND DISCUSSIONS

A. Comparisons to QUAPI

To elucidate the applicability of the CMRT in simulating EET processes, we investigate the EET dynamics of the model dimer system at varying site-energy gap, electronic coupling, exciton-phonon coupling, and temperature. To demonstrate coherent EET dynamics, the artificial initial condition with population localized on site $|1\rangle$, $\sigma(0) = |1\rangle\langle 1|$, is used in all our simulations. A total of 72 sets of parameter combinations were used to compare the dynamical results of the CMRT with the numerically exact QUAPI method.⁴⁰ The QUAPI results we acquired from Pan-Pan Zhang are published elsewhere.⁴⁴ In the following, we verify the accuracy of the CMRT in several representative examples out of the 72 sets of results.

Figure 1 compares the results from CMRT to those from QUAPI in the weak exciton-phonon coupling ($\gamma = 0.2$) regime. Here, we expect CMRT to perform well because the perturbation term is small. Indeed, the results show excellent agreement between CMRT and QUAPI, indicating that CMRT successfully captures coherent EET dynamics. Note that the CMRT correctly describes the coherent oscillations of site populations, which is not considered by the conventional modified Redfield theory.

The success of CMRT in simulating EET dynamics in the intermediate regime is confirmed by comparing the results to those from QUAPI for a model dimer system with $\Delta/\omega_c = 0.5$, $J/\omega_c = 0.5$, and $\gamma = 0.5$ at different temperatures in Fig. 2. The excellent agreement shows that in addition to the applicability in small perturbation cases, the CMRT is also valid in the intermediate regions where the traditional Redfield theory is inadequate.^{9,33,35} Moreover, to investigate the effect of temperature, we show the comparisons at three temperatures in Fig. 2. It shows that the temperature has small influence to the accuracy of the CMRT method in the temperature range that we investigated. It is interesting to note that the overestimation of coherence in the CMRT is

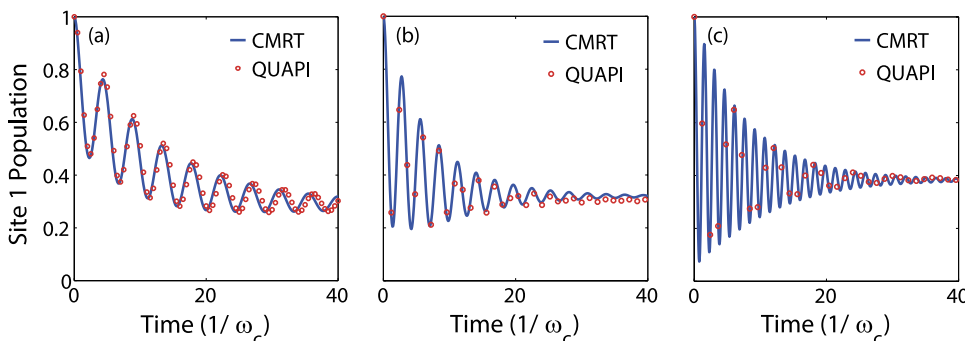


FIG. 1. Comparisons of the EET dynamics simulated by the CMRT and the QUAPI methods in the weak exciton-phonon coupling regions ($\gamma = 0.2$). (a) $J/\omega_c = 0.5$, (b) $J/\omega_c = 1.0$, and (c) $J/\omega_c = 2.0$. Other parameters are $\Delta/\omega_c = 0.5$ and $\beta\omega_c = 1.0$.

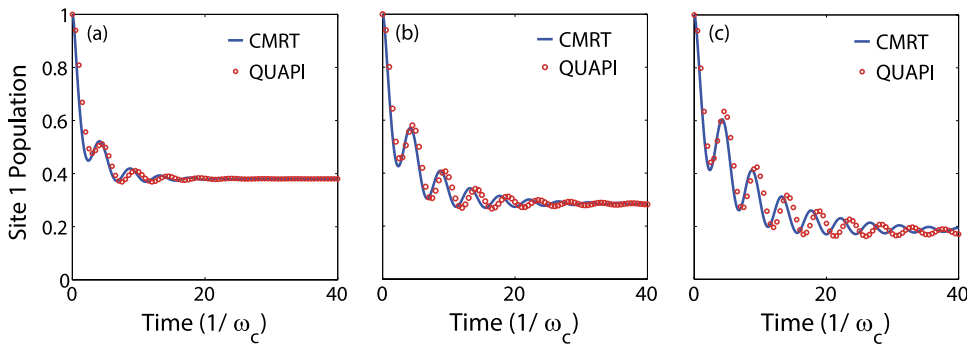


FIG. 2. Comparisons of the EET dynamics simulated by the CMRT and the QUAPI methods in the intermediate regime: (a) $\beta\omega_c = 0.5$, (b) $\beta\omega_c = 1.0$, and (c) $\beta\omega_c = 2.0$. Other parameters are $\Delta/\omega_c = 0.5$, $\gamma = 0.5$, and $J/\omega_c = 0.5$.

clearly seen in Fig. 2(c), where a small overestimation of the coherent oscillation frequency caused by the assumption of a fully delocalized exciton basis is apparent. Besides the slight frequency shift, in this case, the relaxation time and decoherence time are actually well-described by the CMRT method.

Figure 3 shows simulated EET dynamics at strong exciton-phonon couplings ($\gamma = 2.0$) and small site-energy gap ($\Delta/\omega_c = 0.5$), where CMRT actually fails. In Fig. 3, the dynamical results of the CMRT deviate significantly from the exact results calculated by the QUAPI method. Our comparisons show that CMRT often over-estimates the population transfer rate and shows excessive coherence when the bath reorganization energy is larger than the site energy gap. This can be attributed to the over-estimation of the electronic coherence in the fully delocalized exciton basis adopted in the CMRT method. The results confirm the report of Novoderezhkin *et al.*,³⁵ where they concluded that the modified Redfield theory significantly overestimates the transfer rate for systems with small energy gaps and strong electronic couplings.

In the cases where the site-energy gap is large, we found CMRT to provide adequate results regardless of the strength of exciton-phonon couplings. Figure 4 shows the comparison in the large site-energy gap ($\Delta/\omega_c = 2.0$) and intermediate exciton-phonon coupling ($\gamma = 1.0$) cases. As the dimer exhibits a large site-energy gap, the exciton states are rather localized in these cases, and the dynamics become diffusive, showing an incoherent exponential decay characteristics. This is the conventional Förster regime of EET dynamics, and clearly, CMRT performs really well in this parameter regime. In the range of the excitonic couplings (J) studied here, the CMRT is in excellent agreement with the QUAPI. We remark that the

discrepancy between CMRT and QUAPI in Fig. 4(c) could be due to the limited data points supplied in the QUAPI results because of the high computational demand and the high oscillation frequency inherent to the system. The agreement remains excellent even when the exciton-phonon coupling becomes stronger ($\gamma = 2$), as shown in Fig. 5. The excellent performance of CMRT at large Δ , when $J/\Delta < 1$, can be attributed to the inclusion of the diagonal part of the exciton-phonon coupling into the zeroth-order Hamiltonian. This not only reduces the magnitude of the perturbation term but also enables the CMRT to adequately describe multiphonon effects. Energy conservation is a key controlling factor in quantum dynamics. Regarding energy relaxation between two excitons in a molecular system, the excess energy corresponding to the energy gap between the two states must be dumped to the phonon bath. When the energy gap is large and there is a lack of high frequency modes in the bath, a multiphonon transition mechanism will be required for efficient energy relaxation. Therefore, the CMRT has a wider range of applicability in such cases compared to the traditional Redfield theory, which contains only single-phonon dynamics.

The important roles of multiphonon dynamics in EET were discussed by Yang and Fleming.³³ They compared the Förster, traditional Redfield, and modified Redfield theories by simulating EET rates as a function of the energy gap. Their study demonstrated that traditional Redfield theory and modified Redfield theory coincide in cases in which the energy gap between two monomers approaches zero (i.e., a completely delocalized exciton basis). However, at large gaps, the traditional Redfield theory fails to reach the Förster limit, while the modified Redfield theory smoothly interpolates between the two limits. Yang and Fleming emphasized that the lack of phonon reorganization and the neglect of the

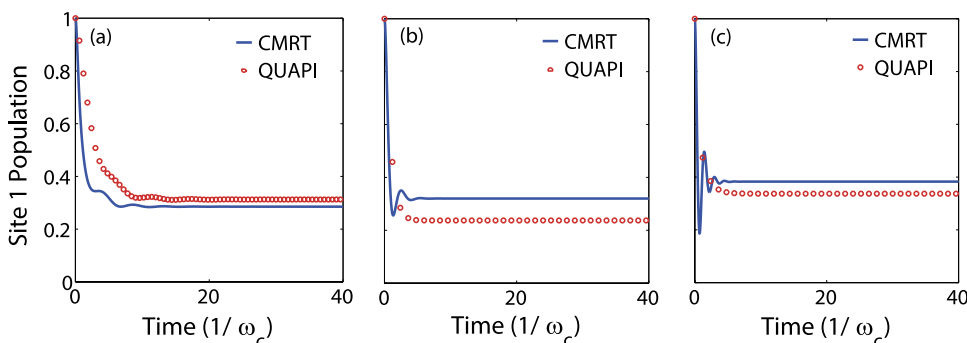


FIG. 3. Comparisons of the EET dynamics simulated by the CMRT and the QUAPI methods at strong exciton-phonon coupling ($\gamma = 2.0$) and small energy gap ($\Delta/\omega_c = 0.5$). (a) $J/\omega_c = 0.5$, (b) $J/\omega_c = 1.0$, and (c) $J/\omega_c = 2.0$. Here, $\beta\omega_c = 1.0$.

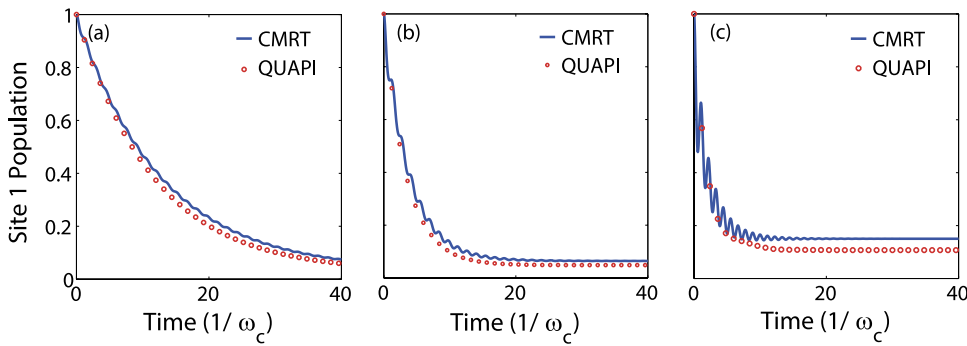


FIG. 4. Comparisons of the EET dynamics simulated by the CMRT and the QUAPI methods at large site-energy gap ($\Delta/\omega_c = 2.0$): (a) $J/\omega_c = 0.5$, (b) $J/\omega_c = 1.0$, and (c) $J/\omega_c = 2.0$. Other parameters are $\gamma = 1.0$ and $\beta\omega_c = 1.0$.

multiphonon effect results in the failure of the traditional Redfield theory in large energy gap regions, evident by the validity of the traditional Redfield theory when applied in a wide spectrum of phonon modes regardless of the strength of electron-phonon couplings. In this regard, the multiphonon process is well captured by the original modified Redfield theory. Our results confirmed that their findings are valid even when the coherent dynamics are considered, and these results yield important physical insights into how exciton-phonon couplings mediate EET dynamics.

In summary, our comparisons of the CMRT and the QUAPI methods indicate that the CMRT performs strongly in a large EET parameter space, except for cases where energy gap is small and exciton-phonon coupling is large. We remark that in the limit where both excitonic couplings (J) and exciton-phonon couplings (γ) are strong, the CMRT could significantly overestimate coherence effects (e.g., Fig. 3), leading to strong and prolonged site-population oscillations in the dynamics. Therefore, we verified through the comparisons of the CMRT with the numerically exact QUAPI method that the CMRT is a promising perturbative approach, which successfully simulates the EET process in a wide range of applications in cases of both small exciton-phonon coupling strength and large site energy gap.

B. Dynamical localization

From the comparisons with QUAPI presented in Sec. III A, we conclude that CMRT delivers excellent results in a large part of the EET parameter space and only fails in the limit when energy gap is small and exciton-phonon coupling is strong. We attribute this to the neglect of dynamical localization in CMRT.

The CMRT is constructed in the exciton basis, which consists of excitonic eigenstates based on constant mean-field electronic couplings. In this representation, exciton states do not depend on strength of exciton-phonon coupling or temperature. However, at large exciton-phonon couplings or high temperatures, dynamical fluctuations in the environments surrounding an excitonic system could destroy coherence between pigments and strongly suppress the degree of delocalization of the photoexcitations.^{45–48} Therefore, the effective electronic coupling, hence the effective delocalization length, should be a function of temperature as well as the strength of exciton-phonon couplings. This so-called “dynamical localization” can be viewed as a phenomenon of wave packet collapsing caused by continuous measurements from the bath, which is more pronounced in systems with strong interactions with their baths. For example, in the B800 and B850 rings of the purple bacterial antenna light-harvesting system II, the collapse of electronic wave packet following the photoexcitation leads to the localization of photoexcitations, which strongly affects the dynamics and spectroscopic signals.⁴⁹ Theoretical approaches have been developed to study dynamical localization,^{11,50} however in general, it is quite challenging to be treated accurately. Various polaronic approaches have been developed to specifically include the bath fluctuation effects by using a phonon-dressed exciton-phonon representation (polarons) as the basis for perturbative treatments, which includes the dynamical localization effects in the zeroth-order Hamiltonian. These polaronic methods are promising, but they can also be quite complicated to be generalized to multi-level systems and applied to spectroscopic problems.^{24–28}

The CMRT assumes coherent exciton basis. In this basis, one assumes that electronic coherence is not affected by

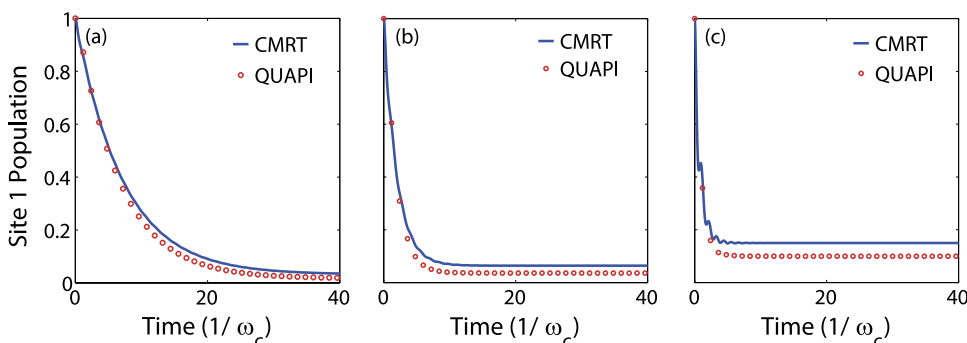


FIG. 5. Comparisons of the EET dynamics simulated by the CMRT and the QUAPI methods at large site-energy gap ($\Delta/\omega_c = 2.0$) and strong exciton-phonon coupling ($\gamma = 2.0$). (a) $J/\omega_c = 0.5$, (b) $J/\omega_c = 1.0$, and (c) $J/\omega_c = 2.0$. Other parameter is $\beta\omega_c = 1.0$.

the strength of exciton-phonon coupling or temperature, effectively neglecting the dynamical localization effect. As a result, electronic coherence is over-estimated in the exciton basis. The neglect of the dynamical localization is not a serious problem when electronic coupling dominates exciton-phonon coupling (where the dynamical localization is small) or when the site-energy gap is large (where the exciton basis is already quite localized). However, it can lead to significant errors in the cases of near isoenergetic levels and large exciton-phonon couplings (Fig. 3), where a small electronic coupling results in fictitious coherently delocalized exciton states that actually should be destroyed by the dynamical fluctuations. When the exciton-phonon interaction is large enough, an overestimation of coherence in small energy gap regions occurs, namely, a phenomenon of having too delocalized basis at large exciton-phonon coupling regions. Therefore, as electronic coupling increases at small site-energy gap systems, errors caused by the overestimation of coherence are amplified (Fig. 3).

So now, we gain a better understanding of why in Fig. 4, the CMRT provides excellent results in large energy gap regions regardless of the strength of electronic couplings. In a highly localized basis case, the phenomenon of overestimated coherence is not significant. Thus, the actual failure of the CMRT and the modified Redfield theory is its neglect of dynamical localization. This concept also explains several minor discrepancies of CMRT when compared to QUAPI. Regarding the temperature effects, since dynamical localization is expected to be more important at higher temperatures, the CMRT is not expected to perform well at high temperatures. It is interesting to note that the temperature dependence in Fig. 2 seems to indicate that CMRT does not perform well in the low-temperature case shown in Fig. 2(c), but, in fact, in this case, CMRT quite accurately reproduced the decoherence time and population transfer time of the QUAPI result. It is a frequency shift (phase shift) of the oscillations, i.e., coherent dynamics, which dominates the deviation. The small frequency shift in the coherent oscillation of the EET population dynamics observed in Fig. 2(c) can be ascribed to the over-estimation of the exciton energy gap due to the neglect of dynamical localization. Because of this delocalized nature in the CMRT, the oscillation of the dynamics is faster than those in the QUAPI. Actually, all the dynamics in Fig. 2 exhibit such overestimation of coherence, and the effect is amplified in the low temperature case shown in Fig. 2(c) due to the longer oscillation time. Moreover, a slight slippage at the equilibrium position of the CMRT results can be apparent especially at large electronic couplings (Figs. 4(c) and 5(c)), which is also attributable to the neglect of dynamical localization. The over-estimation of coherence in CMRT results in exciton states that are too delocalized, leading to equilibrium populations that are closer to 0.5 compared to the QUAPI results. We conclude that the concept of dynamical localization plays an important role in evaluating the theoretical descriptions of EET dynamics, and CMRT fails when the dynamical localization effects are important.

C. Accuracy criteria

Following all the data compiled so far, we aim to develop an accuracy criterion to determine the accuracy of the CMRT under various parameter conditions. A quantitative indicator that can be used to assess the accuracy of an approximated method will be extremely valuable since it can be used to guide the choice of methods and also to reveal physical insights. To this end, we first calculated the magnitude of the second order perturbation as a straightforward indicator for the accuracy of a perturbative approach. For the dimer system considered here, the perturbation term has a single off-diagonal exciton-phonon coupling matrix element (Eq. (3)); therefore, the thermal averaged variance of it, which is denoted as ψ , can be regarded as the magnitude of the second order perturbation. We evaluated ψ to yield

$$\begin{aligned}\psi &= \langle |H_{SB}|^2 \rangle / \omega_c^2 \\ &= \sum_n (C_n^\alpha C_n^\beta)^2 \int_0^\infty d\omega J(\omega) \coth\left(\frac{\beta\omega}{2}\right).\end{aligned}\quad (7)$$

Note that we have divided the strength of perturbation by ω_c^2 to make the indicator ψ unitless. The expression of ψ has simple physical interpretations. The factor in front of the integral in Eq. (7) is an electronic factor determined by the electronic Hamiltonian, and it gives an estimate for the degree of delocalization of the exciton states. For a uniformly delocalized state, this factor is at its maximum, whereas for a fully localized state, its value is zero. The integral term clearly yields the strength of exciton-bath couplings. Thus, the criterion can be established: if $\psi < 1$, we expect the perturbative CMRT method to yield excellent results. For example, Eq. (7) indicates that when the exciton states are localized, the electronic factor will be small, leading to $\psi < 1$ even at large exciton-phonon couplings. This is a direct result of the exciton-phonon Hamiltonian possessing a diagonal form in the localized site basis.

In Fig. 6, we present ψ for the dimer system as two-dimensional plots of the parameters including exciton-phonon coupling, site-energy gap, and electronic coupling. The accuracy criterion is roughly selected as $\psi < 1$; therefore, we have plot lines at $\psi = 1$. In addition, we also used circles to denote points where we have explicitly compared CMRT results to QUAPI results. We have confirmed that the value of ψ is highly correlated with the error of CMRT, and indeed, $\psi < 1$ is an excellent indicator for CMRT to provide accurate EET dynamics. In Fig. 6(a), we plot ψ as a function of J/ω_c and γ for dimer systems with a small site-energy gap ($\Delta/\omega_c = 0.5$), showing that while CMRT is still adequate at a large parameter range, its results quickly deteriorate at large J/ω_c and large γ . Figure 6(a) makes plain the results presented in Figs. 1–3. In addition, Fig. 6(b) shows ψ as a function of Δ/ω_c and γ for dimer systems with $J/\omega_c = 1$. Again, ψ exceeds the threshold value of 1 only at small Δ and large γ , showing the predominant regime where CMRT fails.

Moreover, Figures 6(c) and 6(d) show ψ as a function of J/ω_c and Δ/ω_c for dimers with intermediate ($\gamma = 1$) and strong ($\gamma = 2$) exciton-phonon couplings, respectively. The

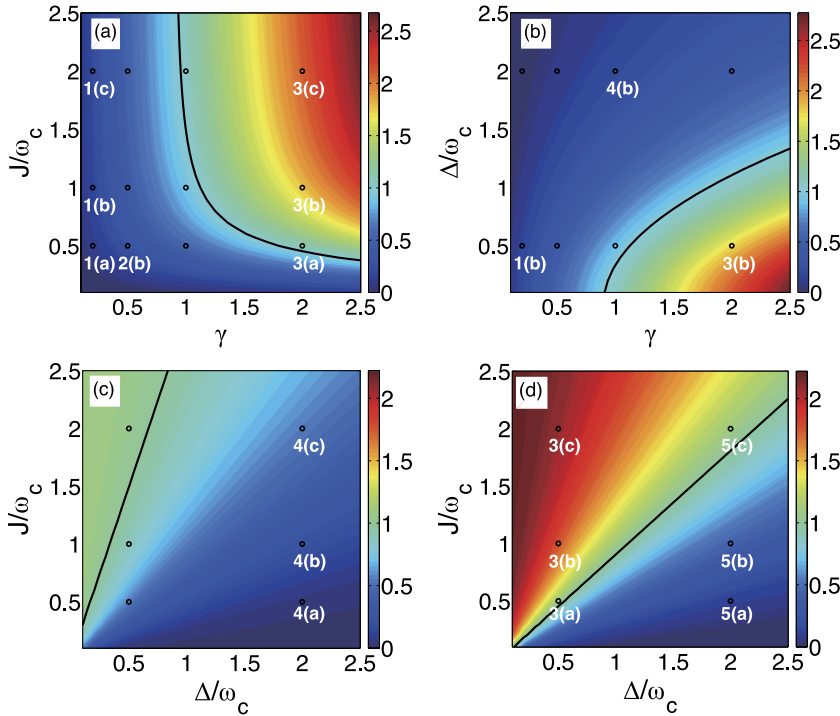


FIG. 6. Magnitude of second order perturbation ψ , which is plotted as functions of (a) exciton-phonon coupling and electronic coupling at $\Delta/\omega_c = 0.5$, (b) exciton-phonon coupling and energy gap at $J/\omega_c = 1.0$, and (c) and (d) site-energy gap and electronic coupling at $\gamma = 1.0$ and 2.0 , respectively. Here, $\beta\omega_c = 1.0$. The black circles represent the parameter points at which the CMRT dynamics were compared with those from the QUAPI method. The solid line is the position where the magnitudes of the accuracy criteria equal to one.

results confirm the validity of CMRT in the intermediate coupling regime and the deteriorated performance as γ increases. Notably, the value of ψ also shows some originally unexpected behaviors that reveal significant physical insights. It is interesting to note that region of large perturbation typically appears in large electronic coupling regions, rather than in small electronic coupling regions. This can be explained by the lack of dynamical localization in CMRT because it overestimates the electronic coherence, which is a problem only when $J/\Delta > 1$. Figures 6(c) and 6(d) clearly show that the ratio J/Δ is also an important factor controlling the accuracy of the CMRT method, and when the electronic coherence is significant (i.e., $J/\Delta > 1$) and the exciton-phonon coupling is strong (Fig. 6(d)), CMRT could yield inaccurate results for EET dynamics.

Furthermore, we found that Eq. (7) can be further simplified for a dimer system in the high-temperature limit. Here, the electronic factor can be related to the site-energy gap (Δ) and electronic coupling (J), and the phonon integral term can be evaluated readily for the spectral density function at the high temperature limit to yield

$$\begin{aligned} \psi' &= \langle |H_{SB}|^2 \rangle / \omega_c^2 \\ &\approx \frac{2J^2}{\Delta^2 + 4J^2} \frac{4\gamma}{\pi\beta\omega_c}. \end{aligned} \quad (8)$$

The physical origins of the magnitude of second-order perturbation are more clearly illustrated in this simplified form. For example, ψ' is proportionally to the exciton-phonon coupling strength γ and the temperature, indicating that the CMRT does not perform strongly under the conditions of large exciton-phonon couplings and high temperatures. In

addition, Eq. (8) clearly reveals a balance between electronic coupling and energy gap. In the Förster limit, where $J/\Delta \ll 1$, ψ' becomes small, suggesting that CMRT performs well in this regime. However, when the energy gap is small, the effect of electronic coupling makes the electronic factor approach a constant (Eq. (8)), and the exciton-phonon coupling strength and temperature become the dominant variables. Therefore, Eq. (8) provides a comprehensive perspective that encompasses results of previous studies on the accuracy of the CMRT method in simulating EET dynamics.

We also compared the simplified high temperature expression ψ' (Eq. (8)) with the full expression ψ (Eq. (7)) in Fig. 7. When the temperature is low (Figs. 7(a) and 7(c)), ψ and ψ' differ in the magnitude, but the structure of the magnitude landscape remains effective the same. Therefore at low temperatures, $\psi' < 1$ is not a appropriate divide for the applicability regime of CMRT, yet it is still an excellent indicator for the accuracy. At high temperatures (Figs. 7(b) and 7(d)), ψ and ψ' coincide; hence, ψ' provides an excellent accuracy criterion.

Besides the magnitudes of second-order perturbation in ψ and ψ' , we have also investigated the ratio between the magnitude of the fourth-order perturbation and the magnitude of the second-order perturbation, $\langle |H_{SB}|^4 \rangle / \langle |H_{SB}|^2 \rangle$, and we found that this factor exhibits exactly the same behavior as ψ in all the parameter range studied. Therefore, ψ and ψ' provide excellent criteria for the accuracy of CMRT in simulating EET dynamics in the parameter range suitable for photosynthetic light-harvesting systems. The results confirm the wide applicability of the CMRT, and the comprehensive study of the accuracy of the CMRT can also assist future applications of the CMRT and point to routes to make improvements to the theory.

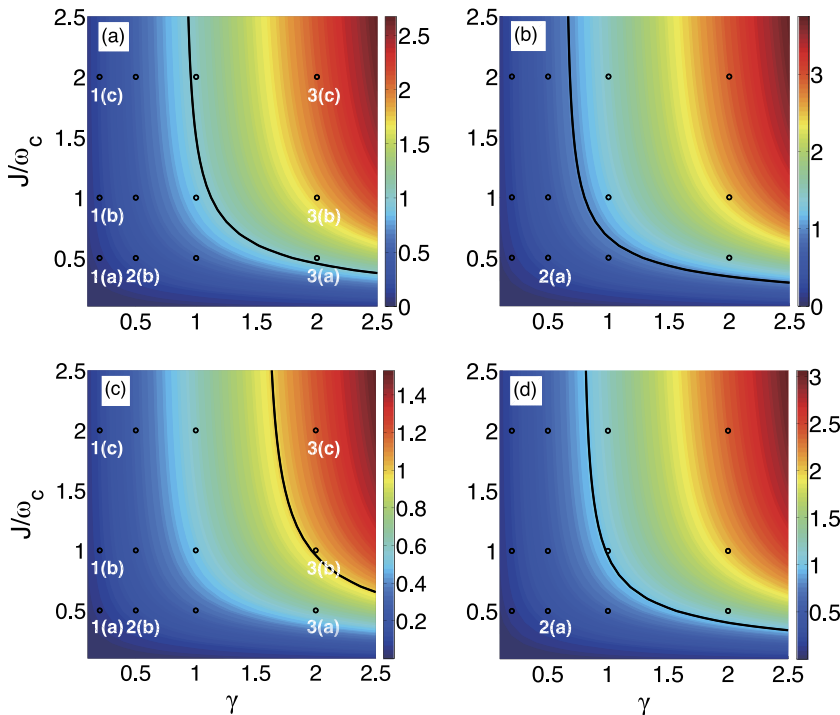


FIG. 7. Magnitudes of second-order perturbation calculated using the full expression (ψ , Eq. (7)) and the high-temperature expression (ψ' , Eq. (8)). (a) ψ at $\beta\omega_c = 1.0$. (b) ψ at $\beta\omega_c = 0.1$. (c) ψ' at $\beta\omega_c = 1.0$. (d) ψ' at $\beta\omega_c = 0.1$. The black circles represent the parameter points at which the CMRT dynamics were compared with those from the QUAPI method. The solid line is the position where the magnitudes of the accuracy criteria equal to one. Here, $\Delta/\omega_c = 0.5$.

D. Comparisons with the small polaron quantum master equation (SPQME)

The established criterion for accuracy enables us to quantitatively compare the performance of different theoretical methods at various parameter regimes. Previously, Chang *et al.*⁴⁴ have investigated EET dynamics in a dimer system by a SPQME approach, which is established based on a small polaron transformation arising from the coupling between the excitonic system and the phonon bath. The polaron transformation dresses the exciton with its surroundings phonons to form “polaron state,” and a theory for EET based on the transformed small polaron basis was first developed by Jang *et al.*²⁴ This SPQME approach also exhibits a broad range of applicability for EET dynamics. It is intriguing to note that the small polaron transformation is expected to over-dress the excitons, leading to an overestimation of dynamical localization effects. This is in contrary to the CMRT method. Therefore, it would be interesting to compare

the valid parameter space of the two methods to examine whether or not they can be complimentary to each other.

Chang *et al.* have also proposed a criterion to assess the accuracy of the SPQME method.⁴⁴ We compare the accuracy criterion for CMRT and that for SPQME in Fig. 8 for a dimer system with small site-energy gap ($\Delta/\omega_c = 0.5$) and low temperature ($\beta\omega_c = 2.0$). The plots show that both methods yield adequate results in a large parameter space; however, their applicable regimes are clearly different. The SPQME performs strongly in the incoherent region where exciton-phonon couplings are relatively large compared with electronic couplings. However, the CMRT is favorable in the region of small exciton-phonon couplings and electronic couplings. Combined, the two theories solved all of the testing cases investigated in this study. The combined results demonstrate that the two theories are complimentary to each other, and this further illustrates the efficacy of using the concept of dynamical localization to characterize the

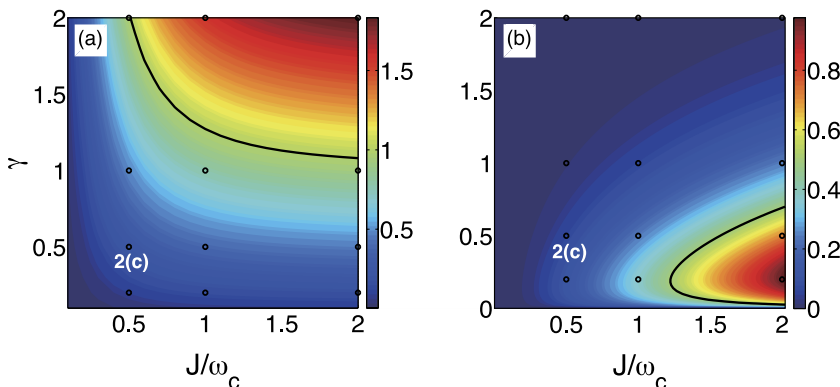


FIG. 8. Comparisons of the accuracy criteria of (a) the CMRT and (b) the SPQME.⁴⁴ The black circles represent the parameter points at which the CMRT dynamics were compared with those from the QUAPI method. The solid line is the position where the magnitudes of the accuracy criteria equal to one. Other parameters are $\beta\omega_c = 2.0$ and $\Delta/\omega_c = 0.5$.

accuracy of methods and the different regimes of EET dynamics. Note that Eq. (8) indicates that CMRT would fail at high temperatures; however, a previous study by Chang *et al.* showed that the SPQME yields excellent results at high temperatures. This further confirms the complementarity of the two methods.

IV. CONCLUSION

In this work, we systematically examined the accuracy of CMRT in a broad parameter regime. The CMRT method is an extension of the modified Redfield theory to treat coherence dynamics in a secular non-Markovian quantum master equation. The CMRT not only provides an efficient and accurate means to simulate EET dynamics but also preserves a clear physical meaning in each term of the equation of motion. The ability to describe quantum coherence dynamics is also a desirable feature in order to explain the experimental observations of coherent EET processes in biological light-harvesting systems.

To demonstrate the wide range of applicability of the CMRT, we calculate the EET dynamics for dimer systems covering a large parameter space for EET and comprehensively compared the results with those from the numerically exact QUAPI method. We conclude that the CMRT performs excellently in most cases. Nevertheless, it can fail in certain regions, in particular, in regions of large exciton-phonon coupling and small site-energy gap. We present a new insight regarding the neglect of dynamical localization in CMRT to explain the poor applicability of the theory in this case. Furthermore, we suggest that the concept of dynamical localization plays a significant role in controlling EET dynamics and the neglect of dynamical localization is the bane of the CMRT method. When the exciton basis states are fairly delocalized, neglecting dynamical localization leads to the overestimation of coherence and significant errors in the EET dynamics. Temperature also plays a role in the performance of the CMRT, which leads to failure at high temperatures.

Furthermore, we propose to assess the accuracy of the CMRT by establishing an accuracy criterion ψ based on the magnitude of second-order perturbation to elucidate the applicability of the CMRT in different parameter regions. We showed that ψ faithfully represents the quality of CMRT results in all the parameter ranges investigated in this study, and $\psi < 1$ serves as an excellent indicator to determine regimes where CMRT provides excellent results. The simple indicator for the accuracy of CMRT provides clear understanding of the physics captured (or not captured) by CMRT. Moreover, we simplified the calculation of ψ with a high temperature approximation. The simplified expression encompassed all the benchmark results of the CMRT and once again emphasized the importance of dynamical localization in the determination of the accuracy of CMRT. Moreover,

the high-temperature expression also provides physical insights into how various parameters affect the performance of CMRT. Therefore, we provide a comprehensive perspective in Eq. (8) that encompasses results of previous studies on the performance of the modified Redfield theory and CMRT; the indicator should not only be useful for assessing the accuracy of the theory but should also facilitate the future improvements and extensions of the CMRT. Finally, we quantitatively compared the performance of CMRT to that of SPQME in a large EET parameter space based on the established criteria. The comparison shows that these two methods are complementary to each other, and accurate simulations of EET dynamics for the full parameter space investigated in this work can be achieved by the combination of them.

It is worth pointing out that we preserve the coherence dynamics and the non-Markovian effect to ensure the accuracy of early time dynamics in the propagation of the CMRT, and we also simplify the master equation by discarding the non-secular terms to improve computational efficiency and stability. Non-secular effects such as coherence-to-coherence transfer and population-to-coherence transfer could change the nature of the EET dynamics; however, for the model system studied in this work, the secular CMRT performs rather well in comparison with the exact QUAPI method. Therefore, for the model systems in a broad parameter range investigated in this work, we believe that the non-secular effects are not important. Note that in order to properly study coherence transfer dynamics, a model system with at least three exciton levels is required, because the dimer system has only one coherence density matrix element. The full equation of motion of the CMRT approach can be made to include all the non-secular terms, so it would be interesting to fully investigate the non-secular effects in the perspective of the CMRT theory in the future. A key issue would be to identify parameter ranges where non-secular effects are important and then investigate whether such non-secular dynamics could influence the quantum efficiency of energy transduction. Another advantage of the secular approximation is that the secular form helps to cure positivity violation problem, which can be critical in the strong exciton-phonon coupling limit.^{37,38} The secular CMRT can be cast into a generalized Lindblad form^{38,51} that indicates the positivity is preserved in the CMRT approach. Nevertheless, based on the excellent performance of the secular CMRT in describing the EET dynamics in a large parameter space, we believe it provides a nice balance between accuracy and computational efficiency for model systems studied here when compared to the more complicated non-secular theory.

Note that a functional unit in photosynthetic membranes or organic materials often contains hundreds or even thousands of chromophores; therefore, it will be extremely desirable to have efficient and accurate methods to calculate the EET dynamics. Our results presented in this work show that

CMRT is an excellent perturbative method for simulating EET dynamics in photosynthetic systems, and while CMRT may fail when both site-energy gap is small and exciton-phonon coupling is strong, the SPQME approach can be adopted instead in this regime. The combination of the two methods could provide efficient and accurate means to simulate EET dynamics for large photosynthetic systems. Noticeable, Novoderezhkin *et al.* have proposed a combined modified Redfield-generalized Förster approach to calculate accurate EET dynamics in photosynthetic light-harvesting systems.^{12,29} Here, our results indicate that a combined CMRT-SPQME approach will achieve this goal yet with the coherence dynamics fully described. This direction of theoretical development might provide novel efficient method for accurate EET dynamics that could eventually be applied to systems with hundreds of sites.

ACKNOWLEDGMENTS

We thank Pan-Pan Zhang for kindly providing the QUAPI data. Y.C.C. thanks the Ministry of Science and Technology, Taiwan (Grant No. NSC 100-2113-M-002-008-MY3), National Taiwan University (Grant No. 103R891305), and Center for Quantum Science and Engineering (Subproject No. 103R891401) for financial support. We are grateful to Computer and Information Networking Center, National Taiwan University for the support of high-performance computing facilities. We are grateful to the National Center for High-performance Computing for computer time and facilities.

APPENDIX: DERIVATION OF THE CMRT QME

The CMRT is based on the reduced density matrix approach for open quantum system dynamics,⁴¹ in which the environmental effects are treated statistically as a thermal bath rather than calculated explicitly with dynamics of each bath degree of freedom. In addition, a product state initial condition as indicated in Eq. (A1) is assumed,

$$\rho(0) = \sigma(0) \otimes \rho_B^{eq}, \quad (\text{A1})$$

where $\rho(0)$ is the full system plus bath density matrix at $t = 0$, which is composed of a system part $\sigma(0)$ and a thermal bath part ρ_B^{eq} . ρ_B^{eq} is the thermalized bath density matrix at the equilibrium of excited-state potential well. In other words, we assume the bath reorganization is rapid:

$$\rho_B^{eq} = \frac{\exp(-\beta H^{ph})}{\text{Tr}_B\{\exp(-\beta H^{ph})\}}. \quad (\text{A2})$$

Instead of working with the full density matrix, we focus on the reduced system density matrix calculated by

$$\sigma(t) = \text{Tr}_B\{\rho(t)\}, \quad (\text{A3})$$

where $\text{Tr}_B\{\cdot\}$ denotes trace over all the bath degrees of freedom, such that the bath part is averaged as a thermal bath attaining equilibrium quickly.

Subsequently, following the modified Redfield theory,³² we treat the off-diagonal part of the exciton-phonon Hamiltonian in the exciton basis as the perturbation, and the diagonal part of the exciton-phonon Hamiltonian is included in the zeroth-order Hamiltonian

$$H^0 = H^{el} + H^{ph} + \sum_{\alpha} H_{\alpha\alpha}^{el-ph}, \quad (\text{A4})$$

$$V = \sum_{\alpha \neq \beta} H_{\alpha\beta}^{el-ph}. \quad (\text{A5})$$

The procedure generates an averaged fluctuation of exciton transition energy induced by the bath and a smaller perturbation term in the off-diagonal part.

Applying the quantum Liouville equation and the technique of second-order cumulant expansion, we derived the following quantum master equation for the time evolution of the reduced density matrix:

$$\begin{aligned} \dot{\sigma}(t) = & \frac{-i}{\hbar} \text{Tr}_B\{[H^0, \sigma(t) \otimes \rho_B^{eq}]\} \\ & - \frac{1}{\hbar^2} \int_0^t d\tau \text{Tr}_B\{[V, [V(-\tau), \sigma(t) \otimes \rho_B^{eq}]]\}. \end{aligned} \quad (\text{A6})$$

In the equation, the first term is related to the zeroth-order Hamiltonian, and the second term describes the dissipation processes caused by the perturbation V . In addition, the trace over bath remains in the first term is the result of pure-dephasing in the exciton basis caused by the diagonal exciton-phonon Hamiltonian in the equation. Note that we preserve the coherence dynamics and the non-Markovian effect to ensure the accuracy of early time dynamics in the propagation of the CMRT. We also simplify the master equation by discarding the non-secular terms, because the secular CMRT is not only sufficient to describe the dynamics in the systems investigated in this work but also significantly reduces the computational cost when compared to the more complicated non-secular CMRT.

1. Coherent dynamics and pure-dephasing

After the insertions of the zeroth-order Hamiltonian and perturbation into the quantum master equation, the first term in Eq. (A6) results into Eq. (A7), which is related only to the zeroth-order Hamiltonian and is responsible for the coherence dynamics,

$$\begin{aligned} \dot{\sigma}^{coh}(t) = & \frac{-i}{\hbar} \sum_{\alpha, \beta} |\alpha\rangle\langle\beta| (\epsilon_{\alpha} - \epsilon_{\beta}) \sigma_{\alpha\beta}(t) \\ & - \frac{i}{\hbar} \sum_{\alpha\beta} |\alpha\rangle\langle\beta| \text{Tr}_B\{(H_{\alpha\alpha}^{ph} + H_{\alpha\alpha}^{el-ph}) \rho_B^{eq} \\ & - \rho_B^{eq} (H_{\beta\beta}^{ph} + H_{\beta\beta}^{el-ph})\} \sigma_{\alpha\beta}(t), \end{aligned} \quad (\text{A7})$$

where the former term describes a process of electronic coherent dynamics driven by the exciton Hamiltonian and the latter term is a pure-dephasing of coherence.

To evaluate the thermal average in Eq. (A7), we further defined a pure-dephasing function, $F_{\alpha\beta}(t)$, using

$$F_{\alpha\beta}(t) = \text{Tr}_B \{ e^{-\frac{i}{\hbar} \tilde{H}_{\alpha\alpha}^{ph} t} e^{-\frac{i}{\hbar} \tilde{H}_{\beta\beta}^{ph} t} \rho_B^{eq} \}, \quad (\text{A8})$$

which evolves the reduced density matrix in the displaced coordinates

$$\sigma_{\alpha\beta}^{coh}(t) = e^{-\frac{i}{\hbar} [(\epsilon_{\alpha} - \lambda_{\alpha\alpha\alpha\alpha}) - (\epsilon_{\beta} - \lambda_{\beta\beta\beta\beta})] t} F_{\alpha\beta}(t) \sigma_{\alpha\beta}(0). \quad (\text{A9})$$

In Eq. (A9), $\lambda_{\alpha\alpha\alpha\alpha} = \sum_n |C_n^\alpha|^4 \lambda_n$ is the reorganization energy of the $|\alpha\rangle$ exciton state. $\tilde{H}_{\alpha\alpha}^{ph}$ defined as $D_\alpha^+ H_{\alpha\alpha}^{ph} D_\alpha$ is derived using a displacement operator, $D_\alpha^+ = e^{-\sum_n \sum_i C_n^\alpha C_{ni}^\alpha \gamma_{ni} (b_{ni} - b_{ni}^\dagger)}$. With the help of the pure-dephasing function $F_{\alpha\beta}(t)$, we evaluated its derivative in time to obtain the pure-dephasing rate, $R_{\alpha\beta}^d$,

$$R_{\alpha\beta}^d(t) = - \sum_n (C_n^\alpha C_n^\alpha - C_n^\beta C_n^\beta)^2 (\dot{g}_n(t) + i\lambda_n), \quad (\text{A10})$$

where $g_n(t) = \int_0^\infty d\omega \frac{J_n(\omega)}{\omega^2} \left\{ \coth\left(\frac{\beta\hbar\omega}{2}\right) [1 - \cos(\omega t)] - i[\sin(\omega t) - \omega t] \right\}$ is the lineshape function for site n .

2. Dissipative dynamics

The second part of Eq. (A6) after the insertion of the perturbation term leads to the dissipation processes,

$$\begin{aligned} \dot{\sigma}^{diss}(t) = & \sum_{\alpha\beta\gamma\delta} |\alpha\rangle\langle\beta| [(\Gamma_{\delta\beta,\alpha\gamma} + \Gamma_{\delta\beta,\alpha\gamma}^*) \sigma_{\gamma\delta}(t) \\ & - \Gamma_{\alpha\gamma,\gamma\delta} \sigma_{\delta\beta}(t) - \Gamma_{\beta\delta,\delta\gamma}^* \sigma_{\alpha\gamma}(t)], \end{aligned} \quad (\text{A11})$$

where $\Gamma_{\alpha\beta\gamma\delta}$ is defined by

$$\Gamma_{\alpha\beta\gamma\delta} = \frac{1}{\hbar^2} \int_0^t d\tau \langle V_{\alpha\beta} V_{\gamma\delta}(-\tau) \rangle_B. \quad (\text{A12})$$

We further simplified the complicated form of Eq. (A11) by applying secular approximation to retain the major changes of density matrix elements during the course of dissipation. As a result, only two processes are considered: the population transfer dynamics ($\alpha = \beta, \gamma = \delta$) and the decoherence dynamics ($\alpha \neq \beta, \gamma = \alpha$, and $\delta = \beta$). Hence, the final form of the simplified equation of motion includes population transfer,

$$\dot{\sigma}_{\alpha\alpha}^{diss}(t) = \sum_\gamma (R_{\alpha\gamma} \sigma_{\gamma\gamma}(t) - R_{\gamma\alpha} \sigma_{\alpha\alpha}(t)), \quad (\text{A13})$$

and population-transfer induced dephasing ($\alpha \neq \beta$),

$$\dot{\sigma}_{\alpha\beta}^{diss}(t) = \sum_f -\frac{1}{2} (R_{f\alpha} + R_{f\beta}) \sigma_{\alpha\beta}(t), \quad (\text{A14})$$

with $R_{\alpha\gamma}$ defined as

$$R_{\alpha\beta}(t) = \frac{2}{\hbar^2} \text{Re} \left[\int_0^t d\tau \langle V_{\beta\alpha} V_{\alpha\beta}(-\tau) \rangle_B \right]. \quad (\text{A15})$$

In addition, the imaginary part of the induced-dephasing term is abbreviated in the calculation because of the insignificant influence on the results. The generalized rate $R_{\alpha\beta}(t)$ can be evaluated explicitly using the following equations:

$$R_{\alpha\beta}(t) = 2\text{Re} \left[\int_0^t d\tau A_\alpha(\tau) F_\beta^*(\tau) V_{\alpha\beta}(\tau) \right], \quad (\text{A16})$$

$$A_\alpha(\tau) = e^{-i(\frac{\epsilon_\alpha}{\hbar} + \lambda_{\alpha\alpha\alpha\alpha})\tau - g_{\alpha\alpha\alpha\alpha}(\tau)}, \quad (\text{A17})$$

$$F_\beta^*(\tau) = e^{-i(\frac{\epsilon_\beta}{\hbar} - \lambda_{\alpha\alpha\alpha\alpha})\tau - g_{\alpha\alpha\alpha\alpha}^*(\tau)}, \quad (\text{A18})$$

$$\begin{aligned} V_{\alpha\beta}(\tau) = & e^{[2(g_{\alpha\alpha,\beta\beta}(\tau) - i\lambda_{\alpha\alpha,\beta\beta}(\tau))] \times [\dot{g}_{\beta\alpha,\alpha\beta}(\tau) \\ & - (\dot{g}_{\beta\alpha,\alpha\alpha}(\tau) - \dot{g}_{\beta\alpha,\beta\beta}(\tau) - 2i\lambda_{\beta\alpha,\beta\beta}) \\ & \times (\dot{g}_{\alpha\beta,\alpha\alpha}(\tau) - \dot{g}_{\alpha\beta,\beta\beta}(\tau) - 2i\lambda_{\alpha\beta,\beta\beta})]}. \end{aligned} \quad (\text{A19})$$

Thus, all the tensor elements needed to propagate dynamics using the CMRT method (Eq. (6)) can be evaluated from the exciton Hamiltonian and spectral densities using Eqs. (A16)–(A19).

¹R. E. Blankenship, *Molecular Mechanisms of Photosynthesis* (Wiley-Blackwell, 2002).

²R. J. Cogdell, A. T. Gardiner, H. Hashimoto, and T. H. P. Brotsudarmo, *Photochem. Photobiol. Sci.* **7**, 1150 (2008).

³G. D. Scholes, G. R. Fleming, A. Olaya-Castro, and R. van Grondelle, *Nat. Chem.* **3**, 763 (2011).

⁴F. Odobel, Y. Pellegrin, and J. Warnan, *Energy Environ. Sci.* **6**, 2041 (2013).

⁵Z. Chen, E. M. Grumstrup, A. T. Gilligan, J. M. Papanikolas, and K. S. Schanze, *J. Phys. Chem. B* **118**, 372 (2014).

⁶G. D. Scholes and G. R. Fleming, *Adv. Chem. Phys.* **132**, 57 (2005).

⁷J. Cao and R. J. Silbey, *J. Phys. Chem. A* **113**, 13825 (2009).

⁸S. Jang and Y.-C. Cheng, *WIREs Comput. Mol. Sci.* **3**, 84 (2013).

⁹A. Ishizaki and G. R. Fleming, *J. Chem. Phys.* **130**, 234110 (2009).

¹⁰A. Olaya-Castro and G. D. Scholes, *Int. Rev. Phys. Chem.* **30**, 49 (2011).

¹¹L. A. Pachon and P. Brumer, *Phys. Chem. Chem. Phys.* **14**, 10094 (2012).

¹²V. Novoderezhkin and R. van Grondelle, *J. Phys. Chem. B* **117**, 11076 (2013).

¹³Y. Tanimura, *Phys. Rev. A* **41**, 6676 (1990).

¹⁴R.-X. Xu and Y. Yan, *Phys. Rev. E* **75**, 031107 (2007).

¹⁵A. Ishizaki and Y. Tanimura, *Chem. Phys.* **347**, 185 (2008).

¹⁶A. Ishizaki and G. R. Fleming, *J. Chem. Phys.* **130**, 234111 (2009).

¹⁷J. Prior, A. W. Chin, S. F. Huelga, and M. B. Plenio, *Phys. Rev. Lett.* **105**, 050404 (2010).

¹⁸P. Nalbach, J. Eckel, and M. Thorwart, *New J. Phys.* **12**, 065043 (2010).

¹⁹J. M. Moix and J. Cao, *J. Chem. Phys.* **139**, 134106 (2013).

²⁰G. Tao and W. H. Miller, *J. Phys. Chem. Lett.* **1**, 891 (2010).

²¹P. Huo and D. F. Coker, *J. Chem. Phys.* **133**, 184108 (2010).

²²J. Moix, J. Wu, P. Huo, D. Coker, and J. Cao, *J. Phys. Chem. Lett.* **2**, 3045 (2011).

²³X. Chen, J. Cao, and R. J. Silbey, *J. Chem. Phys.* **138**, 224104 (2013).

²⁴S. Jang, Y.-C. Cheng, D. R. Reichman, and J. D. Eaves, *J. Chem. Phys.* **129**, 101104 (2008).

²⁵S. Jang, *J. Chem. Phys.* **135**, 034105 (2011).

²⁶D. P. S. McCutcheon and A. Nazir, *J. Chem. Phys.* **135**, 114501 (2011).

²⁷A. Kolli, A. Nazir, and A. Olaya-Castro, *J. Chem. Phys.* **135**, 154112 (2011).

²⁸H.-T. Chang and Y.-C. Cheng, *J. Chem. Phys.* **137**, 165103 (2012).

²⁹V. Novoderezhkin, A. Marin, and R. van Grondelle, *Phys. Chem. Chem. Phys.* **13**, 17093 (2011).

³⁰D. I. G. Bennett, K. Amarnath, and G. R. Fleming, *J. Am. Chem. Soc.* **135**, 9164 (2013).

³¹S. Jang, S. Hoyer, G. Fleming, and K. B. Whaley, *Phys. Rev. Lett.* **113**, 188102 (2014).

³²W. M. Zhang, T. Meier, V. Y. Chernyak, and S. Mukamel, *J. Chem. Phys.* **108**, 7763 (1998).

³³M. Yang and G. R. Fleming, *Chem. Phys.* **275**, 355 (2002).

- ³⁴V. I. Novoderezhkin, M. A. Palacios, H. van Amerongen, and R. van Grondelle, *J. Phys. Chem. B* **108**, 10363 (2004).
- ³⁵V. I. Novoderezhkin and R. van Grondelle, *Phys. Chem. Chem. Phys.* **12**, 7352 (2010).
- ³⁶G. S. Engel, T. R. Calhoun, E. L. Read, T. K. Ahn, T. Mancal, Y.-C. Cheng, R. E. Blankenship, and G. R. Fleming, *Nature* **446**, 782 (2007).
- ³⁷Y.-H. Hwang-Fu, W. Chen, and Y.-C. Cheng, *Chem. Phys.* **447**, 46 (2015).
- ³⁸Q. Ai, Y.-J. Fan, B.-Y. Jin, and Y.-C. Cheng, *New J. Phys.* **16**, 053033 (2014).
- ³⁹Q. Ai, T.-C. Yen, B.-Y. Jin, and Y.-C. Cheng, *J. Phys. Chem. Lett.* **4**, 2577 (2013).
- ⁴⁰M. Topaler and N. Makri, *Chem. Phys. Lett.* **210**, 285 (1993).
- ⁴¹H. P. Breuer and F. Petruccione, *The Theory of Open Quantum Systems* (Oxford University Press, USA, 2002).
- ⁴²A. Suarez, R. J. Silbey, and I. Oppenheim, *J. Chem. Phys.* **97**, 5101 (1992).
- ⁴³Y.-C. Cheng and R. J. Silbey, *J. Phys. Chem. B* **109**, 21399 (2005).
- ⁴⁴H.-T. Chang, P.-P. Zhang, and Y.-C. Cheng, *J. Chem. Phys.* **139**, 224112 (2013).
- ⁴⁵T.-C. Yen and Y.-C. Cheng, *Procedia Chem.* **3**, 211 (2011).
- ⁴⁶A. Gelzinis, D. Abramavicius, and L. Valkunas, *Phys. Rev. B* **84**, 245430 (2011).
- ⁴⁷C. K. Lee, J. Moix, and J. Cao, *J. Chem. Phys.* **136**, 204120 (2012).
- ⁴⁸J. M. Moix, Y. Zhao, and J. Cao, *Phys. Rev. B* **85**, 115412 (2012).
- ⁴⁹A. F. Fidler, V. P. Singh, P. D. Long, P. D. Dahlberg, and G. S. Engel, *Nat. Commun.* **5**, 3286 (2014).
- ⁵⁰P. Huo and D. F. Coker, *J. Phys. Chem. Lett.* **2**, 825 (2011).
- ⁵¹H. P. Breuer, *Phys. Rev. A* **75**, 022103 (2007).